Unsteady Transonic Airfoil Computation Using Implicit Euler Scheme on Body-Fixed Grid

Osama A. Kandil* and H. Andrew Chuang†
Old Dominion University, Norfolk, Virginia

The unsteady Euler equations have been derived for the flow relative motion with respect to a frame of reference that is rigidly attached to the moving airfoil. The resulting equations preserve the conservation form. The grid is generated once by an elliptic solver without any need for dynamic grid computation. An implicit approximately factored finite-volume scheme has been developed and implemented through a fully vectorized computer program. The scheme is based on the spatial approximate factorization of Beam and Warming. Implicit second-order and explicit second- and fourth-order dissipations are added to the scheme. The boundary conditions are explicitly satisfied. The scheme is applied to steady and unsteady transonic rigid-airfoil flows. For forced harmonic airfoil motions, periodic solutions are achieved within the third cycle of oscillation. The results are in good agreement with the experimental data.

Introduction

THE problem of accurate prediction of the unsteady transonic airfoil flows remains a challenging problem to the community of computational fluid dynamics. In addition to the flow complexity due to the mixed subsonic and supersonic regions, the unsteady transonic flow problem includes moving shocks with time-dependent strengths, as well as time-dependent vortex shedding, which originates from shock and separation regions.

The majority of existing work is based on the unsteady transonic small-disturbance (UTSD) theory.[1-5] The UTSD equations are derived under the transonic expansion approximations; hence, they are limited to small disturbances and cannot treat flows with strong shocks or large reduced frequencies. Improved accuracy is obtained by using the unsteady full-potential (UFP) equations,[6-9] which require more computational time. Much as with the UTSD formulation, the UFP formulation suffers from the isentropic flow assumption, which limits the application of UFP equations. Nonisentropic flow corrections of the unsteady potential formulation recently have been added to the UTSD and UFP equations to improve their accuracy for flows with strong shocks.[10,11] The effect of viscosity also has been incorporated by using an integral boundary-layer model.[12-15]

The unsteady Navier-Stokes equations represent the best mathematical model for the unsteady transonic flow since they properly model the shock development and motion, shock/boundary-layer interaction, entropy evolution, and vorticity shedding. The time-accurate solution of the Navier-Stokes equations is computationally expensive because of the need for resolving the flow on a fine grid, particularly when the Reynolds number is large. Solutions of the full Navier-Stokes equations have been presented for a NACA 0015 airfoil at a constant pitch rate in a low-subsonic laminar flow.[16] The numerical solution has been obtained by using an implicit approximate-factorization algorithm[17] on a moving grid. Very recently, the thin-layer Navier-Stokes equations have been solved for unsteady laminar and turbulent transonic flows past a pitching NACA 0012 airfoil and for unsteady low-subsonic flows past a NACA 0015 airfoil at a constant pitch rate.[18] The latter case is the same application considered in Ref. 16. The numerical solution has been obtained by using the flux-vector splitting and the flux-difference splitting methods extended for dynamic meshes.[19] In Ref. 18, it is noted that different turbulence models give different normal-force and pitching-moment coefficients.

Numerical solutions of the unsteady Euler equations are less expensive than those of the unsteady Navier-Stokes equations. For the unsteady transonic flow, the unsteady Euler equations adequately model most of the real flow features, with the exception of viscous effects whenever they are substantial. The Euler equations model shock waves and their motion, entropy increase across shocks and entropy gradient, and vorticity production and convection behind shocks, as can be seen from Crocco's theorem and the inviscid vorticity transport equation. Recently, successful time-accurate solutions of the unsteady Euler equations have been presented for pitching airfoils[19] and wings in transonic flows,[20] and for the rolling oscillation of delta wings—a vortex-dominated flow problem in a locally conical supersonic flows.[21] To the best of our knowledge, Ref. 21 is the first work done for unsteady vortex-dominated flows with shock waves, which is directly applicable to maneuvering delta wings.

In this paper, we present an implicit approximately-factored finite-volume scheme for the time-accurate numerical solution of the unsteady Euler equations of the flow relative motion with respect to an airfoil-fixed frame of reference. The scheme is applied to steady and unsteady transonic flows around a NACA 0012 airfoil. For the unsteady flows, the airfoil is in pitching oscillation about a small and moderate mean angle of attack at a large amplitude. The computational results are compared with the experimental data.

Formulation

The strong conservation form of the unsteady Euler equations of the flow relative motion with respect to a rotating frame of reference is given by[21]

$$\frac{\partial' \rho}{\partial t'} + \nabla \cdot (\rho \bar{V}_r) = 0 \tag{1}$$

$$\frac{\partial' (\rho \bar{V}_r)}{\partial t'} + \nabla \cdot (\rho \bar{V}_r \bar{V}_r + p\bar{\bar{I}}) = -\rho[\dot{\bar{\omega}} x \bar{r} + 2\bar{\omega} x \bar{V}_r + \bar{\omega} x (\bar{\omega} x \bar{r})] \tag{2}$$

$$\frac{\partial' (\rho e_r)}{\partial t'} + \nabla \cdot (\rho h_r \bar{V}_r) = -\rho[\bar{V}_r \cdot (\dot{\bar{\omega}} x \bar{r}) + (\bar{\omega} x \bar{r}) \cdot (\dot{\bar{\omega}} x \bar{r})] \tag{3}$$

Received Nov. 26, 1987; revision received July 20, 1988. © 1988 American Institute for Aeronautics and Astronautics, Inc. All rights reserved.

*Professor, Department of Mechanical Engineering and Mechanics. AIAA Associate Fellow.

†Graduate Research Assistant, Department of Mechanical Engineering and Mechanics. Member AIAA.

where

$$e_r = \frac{p}{\rho(\gamma-1)} + \frac{V_r^2}{2} - \frac{1}{2}|\bar{\omega}x\bar{r}|^2 = e - \bar{V}\cdot(\bar{\omega}x\bar{r}) \tag{4}$$

$$h_r = \frac{\gamma p}{\rho(\gamma-1)} + \frac{V_r^2}{2} - \frac{1}{2}|\bar{\omega}x\bar{r}|^2 = h - \bar{V}\cdot(\bar{\omega}x\bar{r}) \tag{5}$$

In Eqs. (1-5), ρ is the density, $\bar{V}$ the absolute flow velocity, $\bar{V}_r$ the relative flow velocity, p the pressure, $\bar{\bar{I}}$ the identity tensor, r the position vector of a fluid particle with respect to the rotating frame of reference, and γ the ratio of specific heats; $\bar{\omega}$ and $\dot{\bar{\omega}}$ the angular velocity and angular acceleration of the rotating frame of reference, e and h the total energy and total enthalpy per unit mass, and e_r and h_r the energy and rothalpy referred to the rotating frame of reference. The prime refers to the time derivative with respect to the rotating frame of reference. Details of the derivation of Eqs. (1-5) are given by the authors in Ref. 21.

Method of Solution

For a two-dimensional flow around a pitching airfoil, the abstract conservative form of Eqs. (1-3) in terms of the Cartesian coordinates (x',y') of the rotating frame of reference is given by

$$\frac{\partial'\bar{q}_r}{\partial t'} + \frac{\partial'\bar{E}_r}{\partial x'} + \frac{\partial'\bar{F}_r}{\partial y'} = \bar{s} \tag{6}$$

$$\bar{q}_r = (\rho, \rho u_r, \rho v_r, \rho e_r)^t \tag{7}$$

$$\bar{E}_r = (\rho u_r, \rho u_r^2 + p, \rho u_r v_r, \rho u_r h_r)^t \tag{8}$$

$$\bar{F}_r = (\rho v_r, \rho u_r v_r, \rho v_r^2 + p, \rho v_r h_r)^t \tag{9}$$

$$\bar{s} = [0, \rho(\ddot{\alpha}y' + 2\dot{\alpha}v_r + \dot{\alpha}^2 x'), \rho(-\ddot{\alpha}x' - 2\dot{\alpha}u_r + \dot{\alpha}^2 y')$$
$$\rho\ddot{\alpha}(y'u_r - x'v_r - \dot{\alpha}x'^2 + \dot{\alpha}y'^2)] \tag{10}$$

$$e_r = \frac{p}{\rho(\gamma-1)} + \frac{u_r^2 + v_r^2}{2} - \frac{1}{2}\dot{\alpha}^2(x'^2 + y'^2) \tag{11}$$

$$h_r = \frac{\gamma p}{\rho(\gamma-1)} + \frac{u_r^2 + v_r^2}{2} - \frac{1}{2}\dot{\alpha}^2(x'^2 + y'^2) \tag{12}$$

The source terms $\bar{s}$ of Eq. (10) has been written for a pitching motion at an angular velocity and angular acceleration of $\bar{\omega} = \dot{\alpha}\bar{k}$ and $\dot{\bar{\omega}} = \ddot{\alpha}\bar{k}$, where $\alpha(t)$ is the angle of attack. The dimensionless freestream velocity is given by

$$\bar{e}_\infty = \cos\alpha\,\hat{i} - \sin\alpha\,\hat{j} \tag{13}$$

where $\hat{i}$ and $\hat{j}$ are the base unit vectors of the $x'y'$ frame of reference. It should be noticed here that the purpose behind writing the equations in the rotating frame of reference is to eliminate the need for computing the grid motion. Next, we give highlights of the implicit scheme. The scheme is an implicit factored finite-volume scheme based on the spatial approximate factorization of Beam and Warming.[17] Introducing the time-independent body-conformed coordinate system ξ' and η' in the rotating frame of reference, Eqs. (6-10) are transformed to

$$\frac{\partial'\hat{Q}_r}{\partial t'} + \frac{\partial'\hat{E}_r}{\partial \xi'} + \frac{\partial'\hat{F}_r}{\partial y'} = \hat{S} \tag{14}$$

$$\hat{Q}_r = J^{-1}(\rho, \rho u_r, \rho v_r, \rho e_r)^t \tag{15}$$

$$\hat{E}_r = J^{-1}(\rho U_r, \rho u_r U_r + \xi_x' p, \rho v_r U_r + \xi_y' p, \rho U_r h_r)^t \tag{16}$$

$$\hat{F}_r = J^{-1}(\rho V_r, \rho u_r V_r + \eta_x' p, \rho v_r V_r + \eta_y' p, \rho V_r h_r)^t \tag{17}$$

$$\hat{S} = J^{-1}\,\bar{s} \tag{18}$$

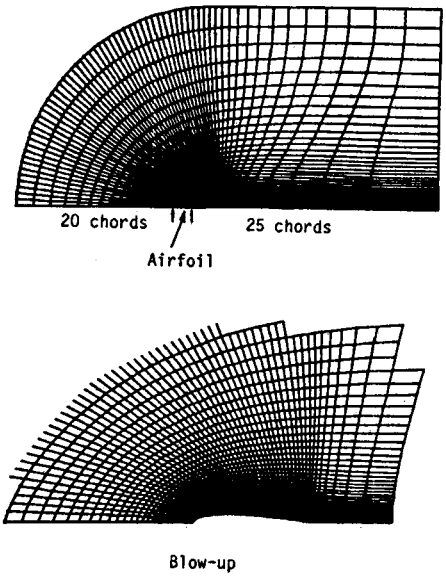

Fig. 1 64 × 128 C grid for NACA 0012.

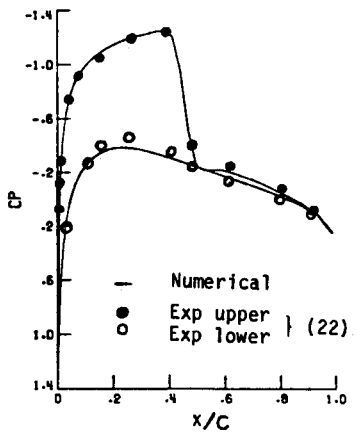

Fig. 2 Surface pressure distribution, NACA 0012, $M_\infty = 0.75$, $\alpha = 2$ deg.

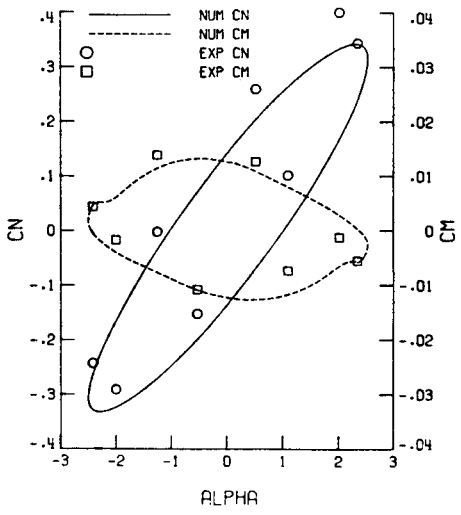

Fig. 3 Lift and pitching-moment coefficients, NACA 0012, $M_\infty = 0.755$, $\alpha_m = 0.016$ deg, $\alpha_0 = 2.51$ deg, $k = 0.0814$, $\Delta t = 0.005$.

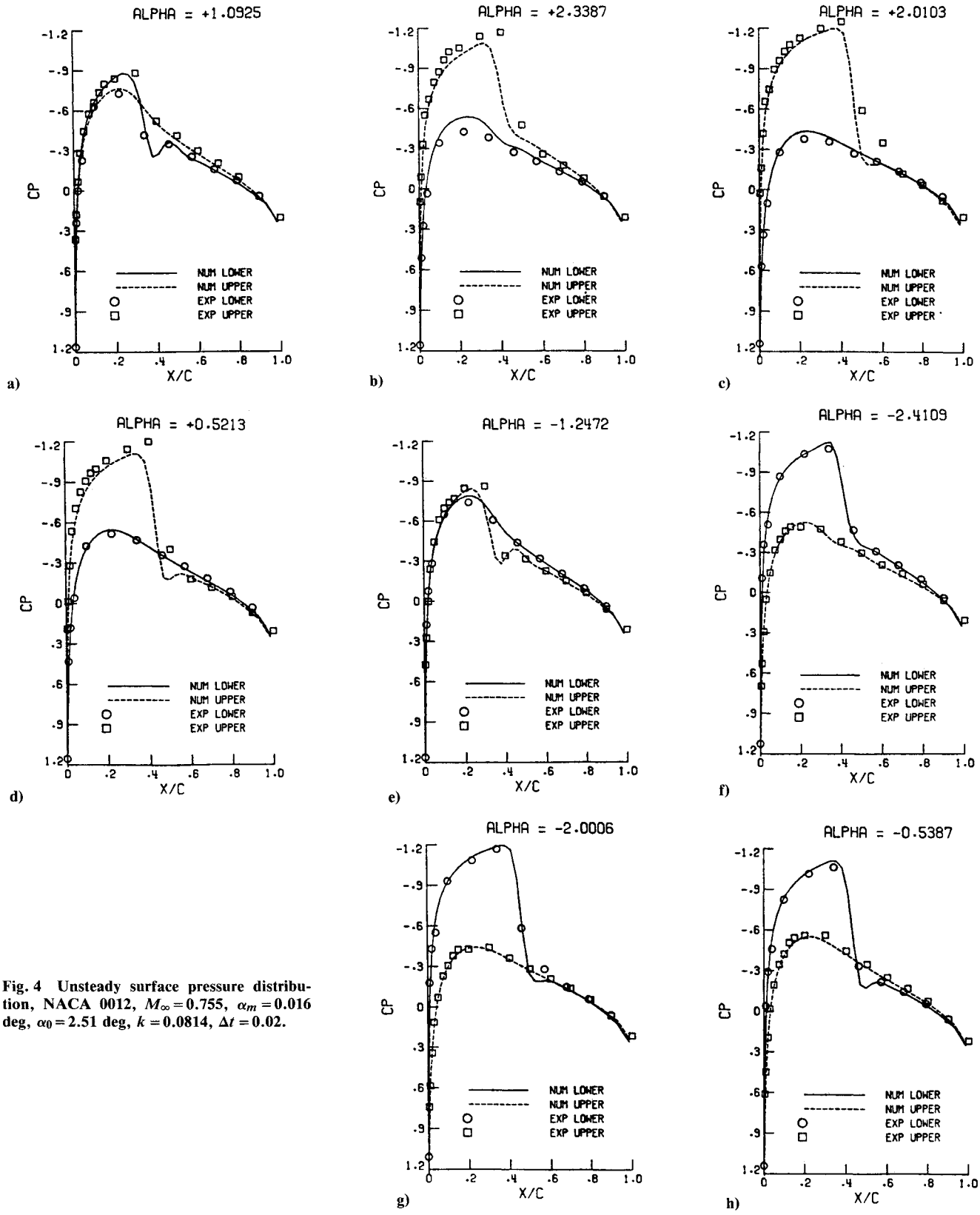

Fig. 4 Unsteady surface pressure distribution, NACA 0012, $M_\infty = 0.755$, $\alpha_m = 0.016$ deg, $\alpha_0 = 2.51$ deg, $k = 0.0814$, $\Delta t = 0.02$.

where

$$\xi' = \xi'(x', y'), \qquad \eta' = \eta'(x', y') \tag{19}$$

$$U_r = \xi_{x'} u_r + \xi_{y'} v_r \tag{20}$$

$$V_r = \eta_{x'} u_r + \eta_{y'} v_r \tag{21}$$

$$J^{-1} = x_{\xi'} y_{\eta'} - x_{\eta'} y_{\xi'} \tag{22}$$

The implicit approximately factored finite-volume scheme of Eq. (14) in the delta form is given by

$$\left(\frac{I}{J\Delta t'} + \delta_{\xi'} A_r^n - \frac{H_r^n}{J} - D_{m\xi'}\right) \times \left(\frac{I}{J\Delta t'} + \delta_{\eta'} B_r^n - D_{m\eta'}\right)$$

$$\times \Delta \bar{q}_r^n = -\frac{1}{J\Delta t'} \bar{W}(\bar{q}_r^n) \tag{23a}$$

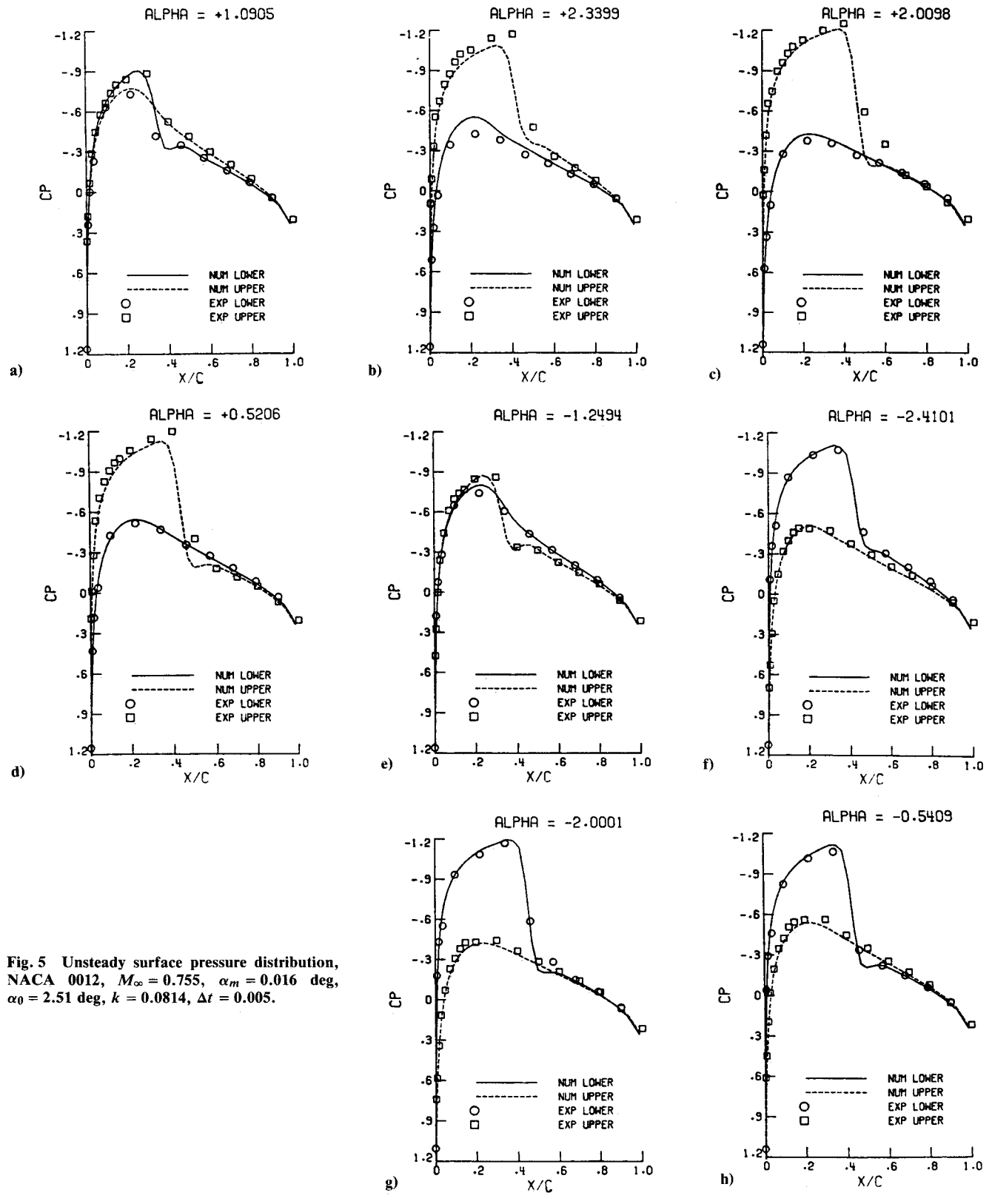

Fig. 5 Unsteady surface pressure distribution, NACA 0012, $M_\infty = 0.755$, $\alpha_m = 0.016$ deg, $\alpha_0 = 2.51$ deg, $k = 0.0814$, $\Delta t = 0.005$.

$$\bar{W}(\bar{q}_r^n) = \hat{E}^n_{r_{i+1/2j}} - \hat{E}^n_{r_{i-1/2,j}} + \hat{F}^n_{r_{i,j+1/2}} - \hat{F}^n_{i,j-1/2} - \hat{S}^n_{i,j}$$

$$- D_{e\xi'}(\bar{q}_r^n) - D_{e\eta'}(\bar{q}_r^n) \tag{23b}$$

where A_r^n, B_r^n, and H_r^n are the Jacobian matrices $\partial\hat{E}_r/\partial q_r$, $\partial\hat{F}_r/\partial q_r$ and $\partial\hat{S}/\partial q_r$, respectively, δ'_ξ and δ'_η the three-point central-difference operators, and D_m and D_e the implicit and explicit dissipation operators, respectively. The implicit dissipation operators are given by

$$D_{m\xi'} = \epsilon_m \frac{I.\ \mathrm{CFL}}{J\Delta t'}(\Delta\nabla)_{\xi'}, \qquad D_{m\eta'} = \epsilon_m \frac{I.\ \mathrm{CFL}}{J\Delta t'}(\Delta\nabla)_{\eta'} \tag{24}$$

where ∇ and Δ are simple backward and forward difference operators, ϵ_m the implicit damping coefficient, and CFL is the Courant-Friedricks-Lewy number. The explicit dissipation operator D_e of Eq. (23) consists of the second- and fourth-order dissipation terms (with damping coefficients of ϵ_2 and ϵ_4),

which have been used earlier in the explicit scheme of Ref. 21. The solution of Eq. (23) is accomplished through two sweeps; one in the ξ' direction and the other in the η' direction. Once this is accomplished, we obtain $\bar{q}_r^{n+1}$ by using

$$\bar{q}_r^{n+1} = \bar{q}_r^n + \Delta\bar{q}_r^n \tag{25}$$

The pressure p then is calculated from Eq. (11).

Boundary Conditions

The surface boundary condition is enforced explicitly through the normal momentum equation

$$\frac{\partial p}{\partial n} = \rho\bar{V}_r \cdot (\bar{V}_r \cdot \nabla\hat{n}) - \rho\hat{n} \cdot \bar{a}_t \tag{26}$$

where

$$\bar{a}_t = \dot{\bar{\omega}} \times \bar{r} + 2\bar{\omega} \times \bar{V}_r + \bar{\omega} \times (\bar{\omega} \times \bar{r})$$

and $\hat{n}$ is the unit normal of the airfoil surface. Also, the far-field boundary conditions are enforced explicitly. In the present application, subsonic flow in the far field is considered and, hence, the inflow-outflow boundary conditions are based on the Riemann invariants R_∞ and R_i for one-dimensional flow normal to the boundary, which are given by

$$R_\infty = \bar{V}_\infty \cdot \hat{n} - \frac{2}{\gamma - 1}(\gamma p_\infty/\rho_\infty)^{1/2} \tag{27}$$

$$R_i = \bar{V}_1 \cdot \hat{n} + \frac{2}{\gamma - 1}(\gamma p_i/\rho_i)^{1/2} \tag{28}$$

where $\hat{n}$ is the unit normal of the outer boundary of the computational region and the subscripts ∞ and i refers to the far-field conditions and the values extrapolated from the interior cells at the boundary, respectively. Thus, the inflow boundary conditions are given by

$$(\bar{V} \cdot \hat{n})_b = \tfrac{1}{2}(R_\infty + R_i) \tag{29a}$$

$$(p/\rho)_b = \frac{1}{\gamma}\left[\frac{\gamma - 1}{4}(R_i - R_\infty)\right]^2 \tag{29b}$$

$$(p/\rho^\gamma)_b = (p/\rho^\gamma)_\infty \tag{29c}$$

$$(\bar{V} \cdot \hat{t})_b = (\bar{V} \cdot \hat{t})_\infty \tag{29d}$$

where b refers to the boundary and $\hat{t}$ is a unit vector tangential to the boundary. For the outerflow boundary conditions, the subscript ∞ in Eqs. (29c) and (29d) is replaced by the subscript i. Equations (29a–29d) give a complete definition of the flow at subsonic boundaries.

The grid is generated by an elliptic solver. Figure 1 shows a typical C grid for the NACA 0012 airfoil with 64 × 128 cells in the lateral direction and around the airfoil, respectively. The computational domain extends 20 chords ahead of the airfoil and 25 chords behind the trailing edge. A blowup of the grid also is shown in Fig. 1. The implicit scheme has been coded through a fully vectorized computer program for the VPS-32 computer of the NASA Langley Research Center.

Computational Results

The implicit computer program has been used to calculate steady and unsteady transonic airfoil flows around a NACA 0012. The implicit and explicit dissipation coefficients have constant values for all the computed cases. Their values are $\epsilon_m = 0.25$, $\epsilon_2 = 0.25$, and $\epsilon_4 = 0.004$. A C grid of 64 × 128 has been used for all the results given here.

Steady Transonic Flow

Several steady transonic airfoil flows have been computed to validate the computer program. Figure 2 shows a sample of the results of the surface pressure for a NACA 0012 at a freestream Mach number, $M_\infty = 0.75$, and at an angle of attack, $\alpha = 2$ deg. This case is computed with a CFL number of 100. The computed results are compared with experimental data taken from Ref. 22. The results are in good agreement with the experimental data, with the exception of the upper surface pressure behind the shock, where the numerical solution shows a stronger shock than the experimental one. Now that we have established confidence in the scheme and the computer program, we next consider unsteady transonic airfoil flows.

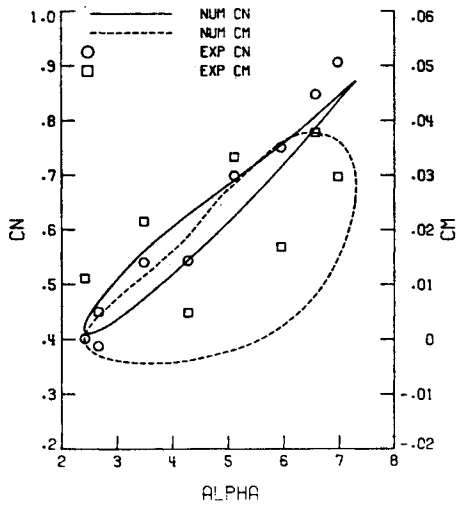

Fig. 6 Lift and pitching-moment coefficients, NACA 0012, $M_\infty = 0.6$, $\alpha_m = 4.86$ deg, $\alpha_0 = 2.44$ deg, $k = 0.081$, $\Delta t = 0.01$.

Unsteady Transonic Flow

Two unsteady transonic airfoil flows have been computed, and the results have been compared with the experimental data of Ref. 23. The airfoil is given a pitching oscillation around an axis at the quarter-chord length. The angle of attack $\alpha(t)$ is given by

$$\alpha(t) = \alpha_m + \alpha_0 \sin[(2\sqrt{\gamma}M_\infty)\, kt] \tag{30}$$

where α_m is the mean angle of attack, α_0 the amplitude, and k the reduced frequency [$= (k^*/U_\infty)(C/2)$, $k^* \equiv$ frequency, $C \equiv$ chord length]. The initial conditions correspond to the steady flow solution at the mean angle of attack α_m.

Figure 3 shows the computed periodic normal force C_N and pitching-moment C_M coefficients for $M_\infty = 0.755$, $\alpha_m = 0.016$ deg, $\alpha_0 = 2.51$ deg and $k = 0.0816$. This case has been computed with a time step $\Delta t = 0.005$. The experimental data[23] of this case also are given in Fig. 3. The computed results show good agreement with the experimental data at several locations of the cycle. The computations also are repeated for the same case using a coarser time step of $\Delta t = 0.02$. No appreciable differences are found when these results are compared with the small time-step results. Figures 4a–4h and 5a–5h show the corresponding computed unsteady surface pressure for $\Delta t = 0.02$ and 0.005, respectively. In these figures the experimental data[23] also are shown. Comparing the surface pressures of Figs. 4 and 5, we notice the slightly smaller shock strengths for $\Delta t = 0.02$. The computed results are in good agreement with the experimental data, with the exception of the results at $\alpha = 1.0925$ deg (Fig. 4a) and at $\alpha = 1.0905$ deg (Fig. 5a) in the range of x/c of 0.1–0.4. It should be noticed that the computed results agree with the experimental data for the corresponding negative angles of attack; $\alpha = -1.2472$ deg (Fig. 4e) and $\alpha = -1.2494$ deg (Fig. 5e). These results raise doubts about the experimental data at $\alpha = 1.0925$ deg (Figs. 4a and 5a).

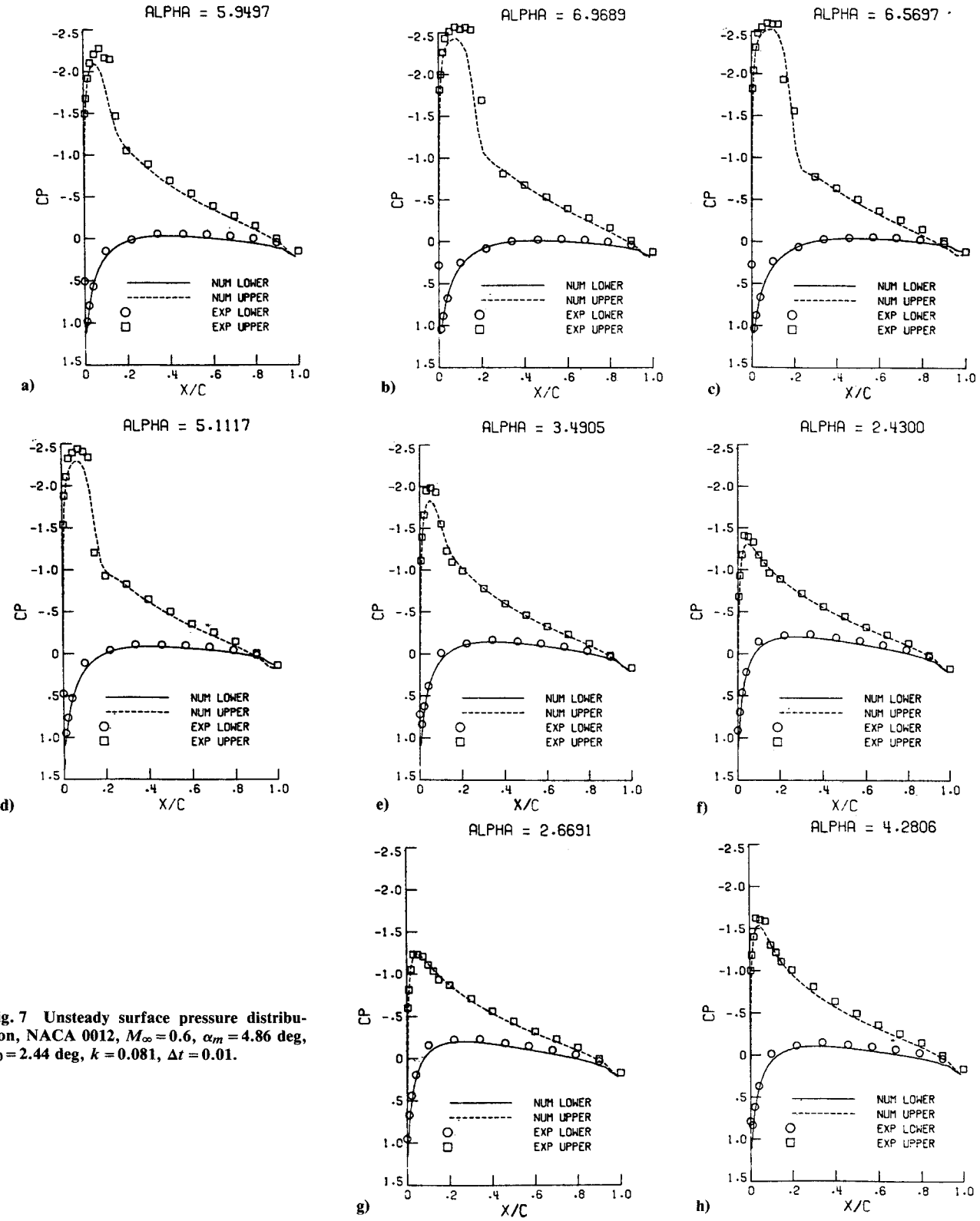

Fig. 7 Unsteady surface pressure distribution, NACA 0012, $M_\infty = 0.6$, $\alpha_m = 4.86$ deg, $\alpha_0 = 2.44$ deg, $k = 0.081$, $\Delta t = 0.01$.

Figure 6 shows the computed periodic normal-force and pitching-moment coefficients, C_N and C_M for $M_\infty = 0.6$, $\alpha_m = 4.86$ deg, $\alpha_0 = 2.44$ deg and $k = 0.081$. This case has been computed with a time step of $\Delta t = 0.01$. The experimental data of this case also are shown in Fig. 4. The computed C_N is in good agreement with the experimental data, with the exception of the high angle of attack range. The computed C_M is lower than that of the experimental data. Figures 7a-7h shows the corresponding computed unsteady surface pressure. For the high angle of attack range, the computed surface pressure is underpredicted at the peak values whereas, for the low angle of attack range, the computed surface pressure is in good agreement with the experimental data. For the high angle of attack range, we attribute the discrepancies to the viscous effects of flow separation and the grid coarseness as well.

The periodic solutions of the two cases just considered have been obtained within the third cycle of oscillation. For $\Delta t = 0.01$ of the second case, each cycle of oscillation takes about 5292 time steps. The computational speed on the VPS-32 averages approximately 1400 s of CPU time/cycle of oscillation. It should be noted here that the Jacobian of the inviscid fluxes has been computed at each time step and that no attempt has been made to freeze these computations for a few time steps.

Concluding Remarks

An implicit approximately factored finite-volume scheme has been presented to obtain the time-accurate solution of the unsteady Euler equations. The unsteady Euler equations have been derived for the flow relative motion around airfoils. The resulting equations preserve the conservation form, and they reduce to the conservative form of the steady flow equations for a uniformly translating airfoil. For rigid airfoils, no dynamic grid computation is needed since the grid is rigidly attached to the airfoil, as can be seen from the formulation. The boundary conditions are explicitly enforced in the present work. The scheme has been applied to steady and unsteady transonic flows around a NACA 0012. The results are in good agreement with the experimental data, with the exception of the high angle of attack range, where the inviscid Euler equations cannot handle smooth surface separation. For the unsteady flows, the use of small time steps slightly improves the shock strength, but it does not change the normal-force or pitching-moment coefficients. The present implicit code is computationally efficient and currently is being extended to treat the three-dimensional, unsteady, transonic vortex flows around sharp-edged delta wings.

Acknowledgment

This research work has been supported by the NASA Langley Research Center under Grant NAG-1-648.

References

[1]Ballhaus, W. F. and Goorjian, P. M., "Implicit Finite-Difference Computations of Unsteady Transonic Flows About Airfoils," *AIAA Journal,* Vol. 15, Dec. 1977, pp. 1728–1735.

[2]Rizzetta, D. P. and Chin, W. C., "Effect of Frequency in Unsteady Transonic Flow," *AIAA Journal,* Vol. 17, July 1979, pp. 779–781.

[3]Edwards, J. W., Bland, S. R., and Seidel, D. A., "Experience with Transonic Unsteady Aerodynamic Calculations," NASA TM-86278, Sept. 1984.

[4]Whitlow, W., Jr., "XTRAN2L: A Program for Solving the General-Frequency Unsteady Transonic Small Disturbance Equation," NASA TM-85723, Nov. 1983.

[5]Goorjian, P. M. and Guruswamy, G. P., "Unsteady Transonic Aerodynamic and Aeroelastic Calculations About Airfoils and Wings," AGARD CP-374, Jan. 1985.

[6]Chipman, R. and Jameson, A., "Fully Conservative Numerical Solutions for Unsteady Irrotational Transonic Flow About Airfoils," AIAA Paper 79-1555, July 1979.

[7]Goorjian, P. M., "Implicit Computations of Unsteady Transonic Flow Governed by the Full Potential Equation in Conservation Form," AIAA Paper 80-0150, Jan. 1980.

[8]Ruo, S. Y., Malone, J. B., and Sankar, L. N., "Steady and Unsteady Full Potential Calculations for High and Low Aspect Ration Supercritical Wings," AIAA Paper 86-0122, Jan. 1986.

[9]Ide, H. and Shankar, V. J., "Unsteady Full Potential Aeroelastic Computations for Flexible Configurations," AIAA Paper 87-1238, June 1987.

[10]Fuglsang, D. F. and Williams, M. H., "Non-Isentropic Unsteady Transonic Small Disturbance Theory," AIAA Paper 85-0600, April 1985.

[11]Whitlow, W., Jr., Hafez, M. M., and Osher, S. J., "An Entropy Correction Method for Unsteady Full Potential Flows with Strong Shocks," NASA TM-87769, June 1986.

[12]Rizzetta, D. P., "Procedures for Computation of Unsteady Transonic Flows Including Viscous Effects," NASA CR-166249, Jan. 1982.

[13]Howlett, J. T., "Efficient Self-Consistent Viscous-Inviscid Solutions for Unsteady Transonic Flow," AIAA Paper 85-0482, Jan. 1985.

[14]Berry, H. M., Batina, J. T., and Yang, T. Y., "Viscous Effects on Transonic Airfoil Stability and Response," *Journal of Aircraft,* Vol. 23, May 1986, pp. 361–369.

[15]Howlett, J. T. and Bland, S. R., "Calculation of Viscous Effects on Transonic Flow for Oscillating Airfoils and Comparisons with Experiment," NASA TP-2731, Sept. 1987.

[16]Visbal, M. R. and Shang, J. S., "Numerical Investigation of the Flow Structure Around a Rapidly Pitching Airfoil," AIAA Paper 87-1424, June 1987.

[17]Beam, R. and Warming, R., "An Implicit Scheme for the Compressible Navier-Stokes Equations," *AIAA Journal,* Vol. 16, April 1978, pp. 393–402.

[18]Rumsey, C. L. and Anderson, W. K., "Some Numerical and Physical Aspects of Unsteady Navier-Stokes Computations Over Airfoils Using Dynamic Meshes," AIAA Paper 88-0329, Jan. 1988.

[19]Anderson, W., Thomas, J., and Rumsey, C., "Extension and Applications of Flux-Vector Splitting to Unsteady Calculations on Dynamic Meshes," AIAA Paper 87-1152, 1987.

[20]Ruo, S. Y. and Sankar, L. N., "Solution of Unsteady Rotational Flow Over Supercritical Wings," AIAA Paper 87-0108, Jan. 1987.

[21]Kandil, O. A. and Chuang, H. A., "Computation of Steady and Unsteady Vortex-Dominated Flows with Shock Waves," *AIAA Journal,* Vol. 26, May 1988, pp. 524–531.

[22]Steger, J. L. and Lomax, H., "Transonic Flow About Two-Dimensional Airfoils by Relaxation Procedures," *AIAA Journal,* Vol. 10, Jan. 1972, pp. 49–54.

[23]Landon, R., "NACA 0012 Oscillatory and Transient Pitching," AGARD R-702, 1982.